applied sciences

MDPI

Article

Comparison of Orbital Reconstructive Effect between Customized Orbital Implants Using Three-Dimensional Printed Templates and Conventional Manual-Bending Implants in Blowout Fracture Surgery

Min-Seo Kwon [1] and Hyun Jin Shin [2,*]

[1] School of Medicine, Konkuk University, Seoul 50529, Republic of Korea; tong6878@gmail.com
[2] Department of Ophthalmology, Research Institute of Medical Sciece, Konkuk University Medical Center, Konkuk University School of Medicine, Seoul 50529, Republic of Korea
* Correspondence: shineye@kuh.ac.kr; Tel.: +82-2-2030-7656

Abstract: The aim of the present study was to determine the orbital reconstructive effect of customized orbital implants using three-dimensional (3D) printed templates compared with conventional manual-bending implants using computed tomography (CT)-based orbital volume measurements. This retrospective study reviewed the medical records and 3D-CT images of 90 patients who underwent medial, inferior, or inferomedial orbital wall reconstruction. The selected patients were categorized into two groups: (1) the 3D group that underwent surgery using 3D-printed customized orbital implant templates and (2) the manual group that received a conventional manual technique to mold the implant. The volume discrepancy (VD) was obtained by subtracting the volume of the contralateral unaffected eye from that of the injured eye. Of the 90 patients, 33 and 57 were divided into the 3D and manual groups, respectively. The volumes on the contralateral unaffected side and on the pre- and postoperative injured sides were 22.5 ± 2.9, 23.7 ± 3.0, and 22.3 ± 2.8 cm^3 (mean ± SD), respectively, in the 3D group, and 21.5 ± 2.5, 22.7 ± 2.8, and 21.2 ± 2.7 cm^3 in the manual group. The postoperative VD did not differ between the 3D (–0.2 ± 0.3 cm^3) and manual (–0.3 ± 0.9 cm^3) groups (p = 0.794). The volume on the postoperative injured side did not differ significantly from that on the contralateral unaffected side in the 3D group, but these did differ significantly in the manual group. Postoperative VD also increased with the preoperative VD in the manual group (Pearson correlation coefficient = 0.548, p = 0.001), whereas there was no such association in the 3D group. The orbital volume restoration effect had superior surgical outcomes for large fractures using the customized orbital implant with 3D-printed templates compared with manual-bending implants.

Keywords: manual bending; three-dimensional printed templates; orbital wall fractures

check for updates

Citation: Kwon, M.-S.; Shin, H.J. Comparison of Orbital Reconstructive Effect between Customized Orbital Implants Using Three-Dimensional Printed Templates and Conventional Manual-Bending Implants in Blowout Fracture Surgery. *Appl. Sci.* **2023**, *13*, 9012. https://doi.org/10.3390/app13159012

Academic Editor: Laura Cercenelli

Received: 11 July 2023
Revised: 31 July 2023
Accepted: 3 August 2023
Published: 6 August 2023

1. Introduction

The orbit is a well-designed and complex structure that protects the ocular globes. Orbital wall fractures are the result of traumatic forces being applied to the globe or surrounding bone [1]. The intricate geometry of the bony orbit makes anatomical reconstruction extremely challenging [2]. These traumas to the orbit may cause enophthalmos, globe dystopia, diplopia, or extraocular movement limitation if precise restoration is not achieved [1,3,4].

Orbital wall fractures are commonly managed through the implementation of implants to restore the integrity of the bony structure. Conventional implants are shaped and bent manually during the surgical procedure. However, accurate bending of orbital implant for achieving precise reconstruction of the orbital wall is time consuming and is highly dependent on the experience of the surgeon [5]. Manual molding and trimming of the implant according to a three-dimensional (3D) fracture shape can be significantly challenging when these procedures are based on two-dimensional (2-D) computed tomography (CT) images, especially for large fractures or when performed by inexperienced surgeons. Inaccurate positioning of implants may also induce the above-mentioned complications [6].

Three-dimensional printing technology has recently come into the spotlight [7–9]. This technology enables surgeons to design orbital implants that closely conform to the shapes and surfaces of individual fracture sites [10]. This can result in better functional and aesthetic outcomes and may reduce the risk of surgical complications, with the latter being particularly important for surgeons with less experience [11,12]. The actual time spent in the operating room could also be reduced since the preoperative planning would be more accurate and detailed, and the implants would be customized to the patient. This can reduce risks associated with prolonged surgeries and anesthesia [13].

In our previous study, we introduced customized 3D-printed orbital implant templates and intraoperatively applied them to patients with orbital wall fractures [8]. Our study provided quantitative evidence demonstrating the highly effective reconstruction of anatomical contours using these templates. The authors of the present study measured orbital volumes to compare the efficacy of customized orbital implants using 3D-printed templates with conventional manual-bending implants in orbital wall reconstruction.

2. Materials and Methods

This single-center, retrospective case–control study was conducted at the Department of Ophthalmology, Konkuk University Medical Center, Seoul, Republic of Korea. The study was performed in accordance with the principles of the Declaration of Helsinki, and its protocol was approved by the institutional review board and ethics committee of Konkuk University Medical Center (approval number: 2022-02-053). We reviewed the medical records and 3D-CT scans images of patients with orbital fractures between June 2014 and December 2022. The inclusion criteria for this study comprised the following: (1) a diagnosis of unilateral medial, inferior, or inferomedial orbital fracture confirmed through preoperative radiological assessment using 3D-CT scans; (2) surgical intervention performed within 2 weeks of the injury; and (3) postoperative evaluation, encompassing clinical outcomes and radiological examinations using 3D-CT scans, conducted within 3 months after the operation. The following exclusion criteria were applied: (1) previous trauma history involving the orbital bones (2), combined surrounding facial bone fractures, (3) bilateral fractures, or (4) follow-up period shorter than 3 months.

Patients were divided into two groups: (1) the 3D group were those treated with the customized 3D-printed orbital implant templates, and (2) the manual group included those who underwent surgery using a conventional manual technique to mold the orbital implant. Postoperative CT scans were obtained immediately after surgery in all patients. Patients received follow-up examinations at 1 week, 1 month, 2 months, and 3 months after surgery, during which diplopia and paresthesia were evaluated.

2.1. Designing of Customized Orbital Implant Templates

Customized orbital implant templates were designed (Anymedi Inc., Seoul, Republic of Korea) and used intraoperatively (Figure 1) [11]. The orbits of the patients, including the fracture sites, were subjected to analysis using Mimics and 3-matic software (Materialise, Leuven, Belgium) to create a virtual 3D orbital implant model of the affected region. The software's surface construction tool was employed to reconstruct the fracture site, mimicking the natural contour of the orbit. Subsequently, a virtual 3D orbital implant model was generated, tailored to precisely fit the shape and surface characteristics of the fracture site. This model was then converted into a stereolithography file. The templates and press were 3D printed using a ProJet 3510 SD device (3D Systems, Rock Hill, SC, USA) at a resolution of 32 μm, employing UV-curable plastic with a wax supporter. Following the removal of the wax supporter through melting, the implant underwent thorough cleaning with isopropanol and was subsequently sterilized using ethylene oxide gas at 55 °C, rendering it ready for intraoperative use.

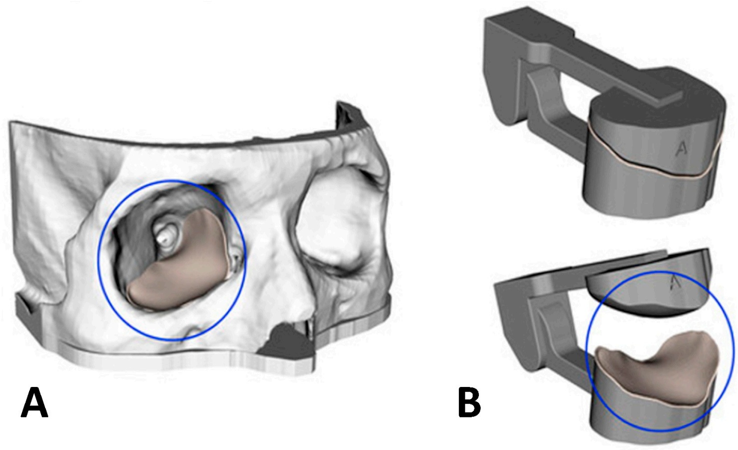

Figure 1. Customized orbital implant templates. A preoperative virtual 3D orbital implant model was created to accurately represent the fracture site (blue circle) (**A**). Subsequently, 3D-printed templates were generated based on the virtual model (**B**).

2.2. Surgical Procedure

After the patients were prepped and draped, a transconjunctival incision was made to approach the inferior or medial wall of the orbit. A periosteal incision and subperiosteal dissection were performed to expose the fracture site. The procedure involved reduction of herniated intraorbital tissue from the orbit. In the control group, the implant was manually trimmed to fit the defect and then inserted into it. In contrast, in the 3D implant group, a customized orbital implant template was used. The template was first traced onto a conventional 2D implant, with all unnecessary portions removed (Figure 2A,B). Subsequently, the implant was positioned between the upper and lower portions of the templates, which were then pressed together while maintaining the axis. This process resulted in the creation of a customized 3D contour on the implant (Figure 2C,D). The conjunctival closure was performed using Vicryl 7-0 sutures. All surgeries were performed by a single surgeon (H.J.S.) using polyethylene with an embedded titanium implant (MEDPOR TITAN, Stryker, Kalamazoo, MI, USA).

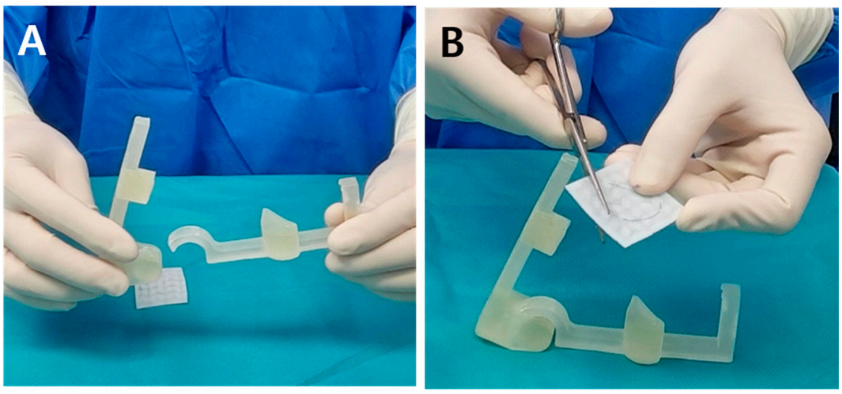

Figure 2. *Cont.*

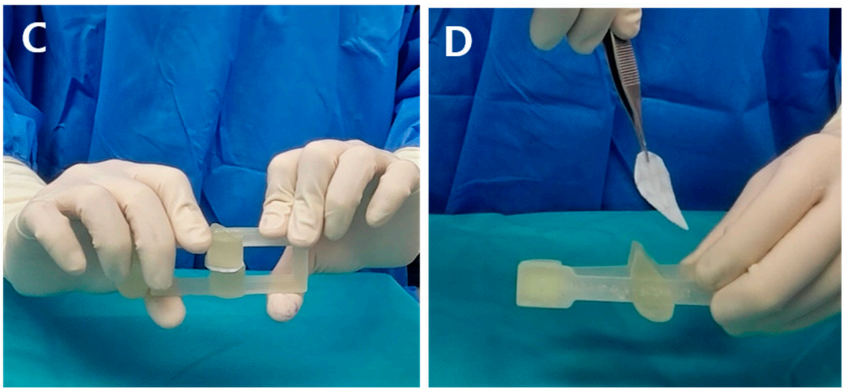

Figure 2. Technique for orbital implant preparation. The upper and lower portions of the templates were designed based on the virtual 3D orbital imaging of the fracture site (**A**). Unnecessary parts of porous polyethylene material containing an embedded titanium implant were carefully cut out (**B**). To create the customized orbital implant, the implant was positioned between the upper and lower portions of the templates, which were subsequently pressed together (**C**). This process ensured the precise formation of a customized 3D contour on the implant (**D**).

2.3. Outcome Measurements

The data were collected during chart review, and included patient demographics (age and sex), pre- and postoperative clinical symptoms (paresthesia and diplopia), and time of operation. Hertel exophthalmometry was used to measure the enophthalmos. Pre- and postoperative orbital volumes were assessed using Mimics and 3-matic software (Materialise). The anterior reference plane was established, and three landmark points were identified on this plane: the supraorbital notch, zygomaticofrontal suture, and the inferior end of the anterior lacrimal crest margin (Figure 3). These landmark points served as crucial reference points for precise measurements of the orbital volumes before and after the surgical intervention. The main outcome measures were the pre- and postoperative orbit volumes of the injured eye, the orbital volume of the contralateral unaffected eye (normal eye), and the orbital volume discrepancy (VD), which was obtain by subtracting the volume of the contralateral unaffected eye from that of the injured eye.

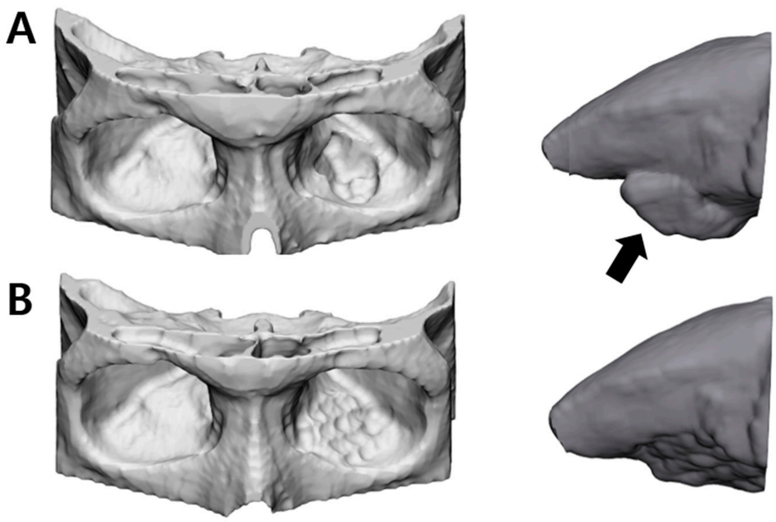

Figure 3. 3D volumetric measurements of the orbital tissue within the bony orbit. Preoperative assessment revealed the presence of herniated orbital tissue through the bony defect of the left orbital floor fracture, as indicated by the arrow (**A**). Following the surgical intervention, a postoperative assessment was performed, and it was observed that the volume of the herniated orbital tissue had markedly reduced (**B**).

2.4. Statistical Analysis

The Statistical Package for the Social Sciences software (version 27.0 for Windows, IBM Corporation, Armonk, NY, USA) was used for statistical analysis. The Shapiro–Wilk test was used to determine whether the data conformed to a parametric (Gaussian) or nonparametric (non-Gaussian) distribution. Mean data were analyzed using the independent *t*-test, and categorical variables were analyzed using the chi-square test. Pre- and postoperative volume changes were compared using the paired *t*-test. The linearity of relationships between the pre- and postoperative VDs was evaluated using the Pearson correlation coefficient. Significance was set at $p < 0.05$.

3. Results

The study included 90 patients aged 41.4 ± 16.2 years (mean ± SD). The comparative analysis was performed on 33 patients who underwent orbital wall reconstruction using 3D-printed customized orbital implant templates and 57 controls who underwent the reconstruction using conventional implant methods. The baseline characteristics and demographic data of the patients are listed in Table 1. There were no intergroup differences in age, sex, operation time, fracture site, defect size, or pre- and postoperative exophthalmometry. In the 3D group, seven of the thirty-three patients complained of diplopia before surgery, while only two complained of diplopia after surgery. In the manual group, eleven of the fifty-seven patients complained of diplopia before surgery, while five complained of diplopia after surgery. In the 3D group, five of the thirty-three patients complained of paresthesia in the injured area before surgery, while four complained of paresthesia after surgery. In the manual group, ten of the fifty-seven patients complained of paresthesia in the injured area before surgery, while seven complained of paresthesia after surgery.

Table 1. Characteristics of the study groups Data are mean ± SD or n (%) values.

Characteristic	3D Group	Manual Group	*p*
Number of patients	33	57	
Age, years	42.0 ± 16.5	36.2 ± 15.8	0.676 [a]
Sex, male/female	22/1	47/10	0.383 [b]
Side, right/left	17/16	22/35	0.414 [b]
Cause of injury			
Fall	0	1	
Assault	13	9	
Accidental bump	18	46	
Traffic collision	2	1	
Fracture site			0.071 [c]
Inferior wall	14 (42.4)	23 (40.4)	
Medial wall	12 (36.3)	22 (38.6)	
Inferiomedial and wall	7 (21.2)	12 (21.1)	
Defect size, cm^2	4.53	4.75	0.459 [a]
Operation time, minutes	61.1 ± 20.5	59.3 ± 18.5	0.881 [a]
Exophthalmometry			
Contralateral unaffected eye	13.7 ± 3.0	13.7 ± 2.3	0.546 [b]
Injured eye, preoperation	13.1 ± 2.9	13.2 ± 2.4	0.525 [b]
Injured eye, postoperation	14.0 ± 2.5	14.1 ± 2.4	0.635 [b]
Preoperative symptoms			
Diplopia	7 (21.15)	11 (19.3)	0.956 [b]
Paresthesia	5 (15.1%)	10 (17.5)	0.769 [b]
Postoperative symptoms			
Diplopia	2 (6.0)	5 (8.8)	0.643 [b]
Paresthesia	4 (12.1)	7 (12.3)	0.982 [b]

[a] Independent *t*-test, [b] chi-square test, [c] chi-square test for trend.

The mean volumes of the contralateral unaffected side, and pre- and postoperative injured sides were 22.5 ± 2.9, 23.7 ± 3.0, and 22.3 ± 2.8 cm^3, respectively, in the 3D group, and 21.6 ± 2.5, 22.7 ± 2.8, and 21.2 ± 2.7 cm^3 in the manual group. The pre- and postoperative VD were 1.1 ± 1.2 and −0.2 ± 0.8 cm^3, respectively, in the 3D group, and

1.2 ± 0.9 and −0.3 ± 0.9 cm^3 in the manual group. No variable was significantly different between these two groups (Table 2).

Table 2. Quantitative comparisons between the two study groups.

	3D Group	Manual Group	p [a]
Orbital volume, cm^3			
(1) Contralateral unaffected eye	22.5 ± 2.9	21.6 ± 2.5	0.162
(2) Affected eye			
Preoperation	23.7 ± 3.0	22.7 ± 2.8	0.583
Postoperation	22.3 ± 2.8	21.2 ± 2.7	0.4310
(3) Comparisons			
Preoperative VD	1.1 ± 1.2	1.2 ± 0.9	0.141
Postoperatice VD	−0.2 ± 0.8	−0.3 ± 0.9	0.794

VD, orbital volume discrepancy which was obtained by subtracting the volume of the contralateral unaffected eye from that of the injured eye. [a] Independent *t*-test.

The volumes on the preoperative lesion side were significantly larger than those on the contralateral unaffected or postoperative injured sides within each group. The volumes on the postoperative injured side did not differ significantly from those on the unaffected contralateral side in 3D group, but they did differ significantly from those on the unaffected contralateral side in the manual group (Table 3). We also found a positive association between pre- and postoperative VDs in the manual group (Pearson correlation coefficient = 0.548, p = 0.001) (Figure 4). In accordance with an increase in preoperative VD, the postoperative VD worsened in the manual group, whereas there was no association between them in the 3D group.

Table 3. Surgical outcomes: within-group comparisons of variables.

Variable	p [a]
Orbital volume of 3D group	
Contralateral unaffected side vs preoperative injured side	**0.001**
Contralateral unaffected side vs postoperative injured side	0.178
Preoperative injured side vs postoperative injured side	**0.001**
Orbital volume of manual group	
Contralateral unaffected side vs preoperative injured side	**0.001**
Contralateral unaffected side vs postoperative injured side	**0.042**
Preoperative injured side vs postoperative injured side	**0.001**

[a] Paired *t*-test; significant p values are in boldface.

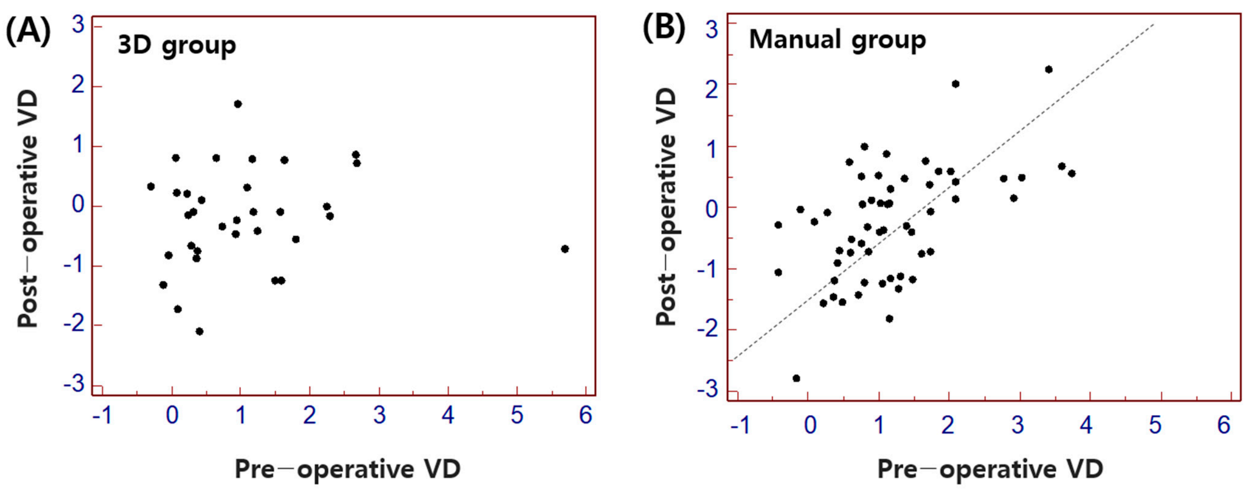

Figure 4. Correlation between pre- and postoperative VDs. (**A**) There was no association between pre- and postoperative VDs in the 3D group. (**B**) A significant positive correlation was observed between pre- and postoperative VDs in the manual group (r = 0.548, p = 0.001).

4. Discussion

The precise restoration of the fractured orbital structure plays a crucial role in achieving both the restoration of the normal structure and volume without any aesthetic or functional complications. This restoration necessitates accurate reformation of the orbit and proper spatial positioning of the globe [14]. However, accomplishing the restoration of the premorbid bony contour [10,14] presents a challenging task due to the intricate 3D nature of the orbit. Even a minor alteration in orbital volume can lead to significant enophthalmos [15–17]. An inadequately positioned orbital implant can result in diplopia and ocular movement restriction caused by entrapment of the extraocular muscle and soft tissue (Figure 5).

The use of 3D printing technology was postulated to enable more precise molding compared with conventional implants. Considering this, the present study aimed to determine the clinical efficacy of personalized orbital implants using a 3D-printed template for orbital volume reconstruction. The volume on the postoperative injured side did not differ significantly from that on the contralateral unaffected side in the 3D group, but these did differ significantly in the manual group. A large orbital fracture also tended to be undercorrected in the manual group, while preoperative fracture size did not affect the postoperative orbital volumes of the restorations in the 3D group (Figure 4). Considering that the orbital volumes on the contralateral unaffected, preoperative, and postoperative injured sides did not differ significantly in both groups (Table 2), the surgical outcome of the 3D group was superior.

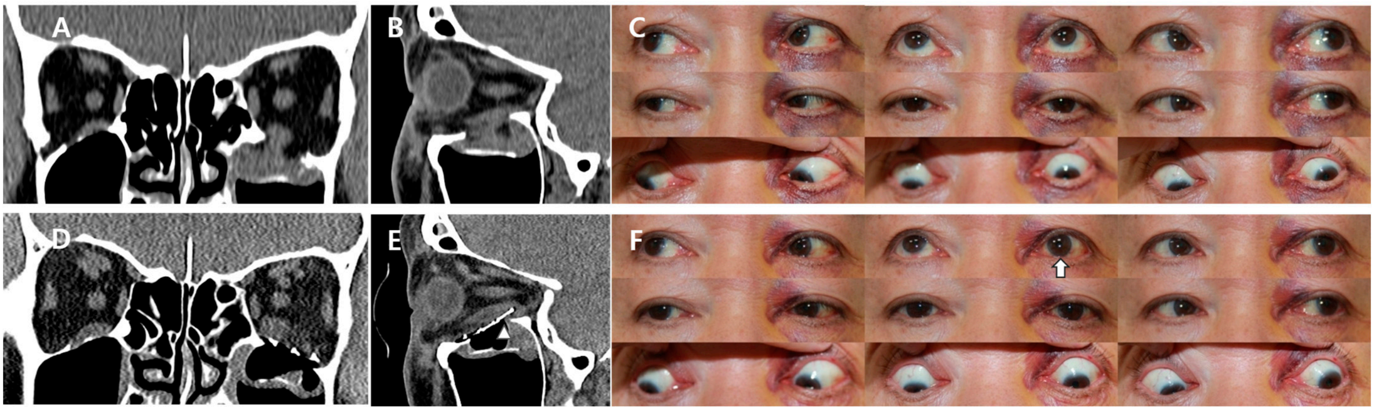

Figure 5. The preoperative facial bone CT images and nine-gaze photographs of 57-year-old male patient who underwent left inferior blowout fracture surgery using the conventional manual technique (**A**–**C**). Despite the positive outcome in terms of orbital volume restoration, immediate postoperative images (**D**–**F**) reveal that the posteriorly misaligned orbital implant compressed the inferior rectus muscle (arrowhead, (**E**)), which restricted the elevation of the left eye (arrow, (**F**)).

The findings of the current study were consistent with the previous research, which also highlighted the effectiveness of the 3D-printed implant in restoring orbital volume. Recent studies found that using 3D-printed implant surgery resulted in a significantly greater volume reduction compared with conventional manual bending methods [18,19]. Those authors concluded that 3D-printed implants for orbital bone fracture reconstruction led to better outcomes by achieving accurate anatomical reconstruction. Moreover, the improved fit and reduced need for tissue handling could have the additional benefit of reducing postoperative edema risk [20].

By utilizing 3D printed templates, the risk of intraoperative implant deformation or errors related to manual bending can be reduced (Figure 5). They conform to the individual anatomy of the patient and could potentially lead to improved aesthetic and functional outcomes, such as improved ocular alignment and reduced risk of complications such as implant migration or extrusion. This result could benefit quality control and potentially lead to more predictable surgical outcomes and safer procedure.

The 3D implant can also be a valuable tool for surgical training [21,22]. Surgeons, especially those with less experience of complex procedures such as orbital fracture repair, can practice their accuracy in trimming and molding of orbital implants by observing 3D implants manufactured according to specific dimensions of different patients. The 3D implants can also compensate for the lack of experience as a patient-specific surgical guide. This allows them to reduce their learning curve and refine their techniques and helps to improve surgical outcomes regardless of fracture size and surgeon's experience.

The use of a customized 3D-printed template can reduce the time spent on intraoperative manipulation and adjustment of the implant to fit the defect, since it would have been designed to fit precisely [20,23]. This can decrease the total surgery time, which can in turn reduce the risks associated with longer surgical procedures including infection or anesthesia complications. Furthermore, streamlined surgical process may contribute to better overall surgical efficiency. Previous studies found that using 3D-printed implants reduced surgical times from an average of 93.3 min with standard implants to 48.3 min [20]. However, our study did not identify any significant difference in surgical times between the two methods. The fracture size and shape were analyzed using CT scanning before surgery in the manual group of the present study. If the preoperative analysis time (10 min) of the implant using CT scans was accounted for, the operation time would be longer in the manual group than in the 3D group, which was consistent with the findings of previous studies.

The volumes of the fractured orbits of all cases in the present study, and the contralateral orbit volume were $23.04 \pm 2.95\,cm^3$ and $21.88 \pm 2.74\,cm^3$. A previous study [24] that used the Eclipse Treatment Planning System (version 13.0, Varian Medical Systems, Palo Alto, CA, USA) to measure orbital volume in patient with blowout fracture obtained results similar to those in our study. That study determined that the volume was $23.01 \pm 2.60\,cm^3$ for the fractured orbits and $21.31 \pm 2.50\,cm^3$ for the contralateral orbits. Orbital volume is typically considered to be smaller in females than in males and smaller in children than in adults [25]. However, there were no differences in age or sex between the two groups in the present study. The previous findings imply that our orbital volume measurements were performed accurately and were free from potential bias related to age and sex, thereby enhancing their reliability.

Several types of 3D printing technology exist, including direct 3D printing and 3D-printed standardized implants. However, the direct printing technique is currently expensive, time consuming, and requires specific equipment. The choice of implant material also remains restricted to titanium. Population-based pre-bent standardized implants have indeed shown superior outcomes compared with conventional-plane 2D implants (as indicated in references [2,26]). Nonetheless, these methods have their limitations as they are unable to fully exploit the potential of 3D printing technology to fabricate entirely personalized implants. This is due to the fact that individual patients possess distinct orbital morphologies, necessitating a more tailored approach to implant design and manufacturing.

The orbital implant template method we present here has several advantages over existing technologies. We placed the implants between the upper and lower portions of the templates, and applied pressure to mold them into the desired shape (Figure 2). First, using a 3D-printed template based on patient-specific imaging data is potentially more accurate than using pre-bent implants based on population averages that are highly unlikely to exactly match the anatomy of each patient. Second, Kang et al. found that the 3D-printed template method has advantages of a shorter manufacturing time and lower cost [11]. The 3D-printed mold costs around US$100, which is much cheaper than the cost of US$3700–6200 for direct 3D printing [12]. Third, our method does not require any specialized equipment, with a standard 3D printer being sufficient. Indeed, the adaptability of the 3D template printing method is a significant advantage, especially in developing countries, as it allows for easy implementation. Any clinic equipped with a 3D printer and suitable software can readily adopt this technology. Finally, this approach offers flexibility to surgeons, as they have the option to choose their preferred commercial implants when utilizing the 3D template printing method. Implants consisting of a mixture of two or more materials, such as the porous polyethylene with embedded titanium implants, are difficult to manufacture using direct 3D printing.

In addition to 3D printing technology, the use of intraoperative navigation surgery utilizing 3D CT prove to be valuable tools in the identification of current implant positions and the confirmation of immediate postoperative orbit status, particularly in the context of complex orbital fractures [27,28]. The synchronous positioning of instruments with 3D CT images offers a valuable approach, allowing for precise and safe surgery on orbital fractures, especially those located around the optic canal. Visualizing the locations indicated by the intraoperative navigation pointer enhances the accuracy and safety of the surgical procedure. In the future, it is essential to conduct studies comparing the effectiveness of surgery that combines implants using 3D printing technology and 3D navigation during surgery with conventional methods in correcting fractures and reducing complications. Such research will provide valuable insights into the potential benefits and advantages of utilizing these advanced techniques in fracture correction and surgical outcomes.

One of the limitations of the present study was its retrospective design, as opposed to being a randomized controlled trial. Second, the number of patients differed between the groups. This difference might have an impact on the standard deviation of the results. Third, postoperative orbital CT scans were conducted immediately after surgery. However, Wi et al. [24] reported that there was no considerable alteration in orbital volume when comparing measurements taken immediately after surgery to those taken during a final follow up at a minimum of 6 months after orbital wall reconstruction. This suggests that the postoperative orbital tissue volume within the bony orbit is unlikely to undergo any clinically significant changes, regardless of the duration of the follow-up period. In this study, we evaluated pre- and postoperative orbital volume but did not analyze qualitative metrics such as pain. Future prospective studies should explore pain and swelling reductions with 3D implants for a more comprehensive understanding of their benefits in orbital wall fracture surgery.

5. Conclusions

Orbits reconstructed using a 3D-printed template method provide better outcomes than using conventional manual-bending implants based on quantitative evaluations of orbital volumes before and after surgery. We believe that customized orbital implants constructed using 3D-printed templates allow for more predictable surgical outcomes because they provide personalized treatment approaches based on individual orbital morphology, address the complexity of fractures more effectively, ensure accurate implant shape and size matching the patient's anatomy, and assist surgeons with precise guides, resulting in consistent and successful outcomes regardless of their skill level.

Author Contributions: Conceptualization, H.J.S.; methodology, M.-S.K.; software, M.-S.K.; validation, H.J.S.; formal analysis, M.-S.K.; investigation, M.-S.K.; data curation, H.J.S.; writing—original draft preparation, M.-S.K.; writing—review and editing, H.J.S.; visualization, M.-S.K.; supervision, H.J.S.; project administration, H.J.S.; funding acquisition, H.J.S. All authors have read and agreed to the published version of the manuscript.

Funding: This work was supported by a National Research Foundation of Korea (NRF) grant funded by the Korea government (MSIT) (no. RS-2023-00251281).

Institutional Review Board Statement: The study was conducted in accordance with the Declaration of Helsinki, and approved by the Institutional Review Board of Konkuk University Medical Center (registration number: 2022-02-053).

Informed Consent Statement: The requirement for informed consent was waived due to the retrospective nature of the study.

Data Availability Statement: Data available on request due to restrictions, e.g., privacy or ethical. The data presented in this study are available on request from the corresponding author. The data are not publicly available because it contains processed patient information.

Conflicts of Interest: The authors declare no conflict of interest. The funders had no role in the design of the study; in the collection, analyses, or interpretation of data; in the writing of the manuscript; or in the decision to publish the results.

References

1. Strong, E.B.; Kim, K.K.; Diaz, R.C. Endoscopic approach to orbital blowout fracture repair. *Otolaryngol.—Head Neck Surg.* **2004**, *131*, 683–695. [CrossRef] [PubMed]
2. Metzger, M.C.; Schon, R.; Weyer, N.; Rafii, A.; Gellrich, N.C.; Schmelzeisen, R.; Strong, B.E. Anatomical 3-dimensional pre-bent titanium implant for orbital floor fractures. *Ophthalmology* **2006**, *113*, 1863–1868. [CrossRef] [PubMed]
3. Joseph, J.M.; Glavas, I.P. Orbital fractures: A review. *Clin. Ophthalmol.* **2011**, *5*, 95–100. [CrossRef] [PubMed]
4. Shin, J.W.; Lim, J.S.; Yoo, G.; Byeon, J.H. An analysis of pure blowout fractures and associated ocular symptoms. *J. Craniofacial Surg.* **2013**, *24*, 703–707. [CrossRef] [PubMed]
5. Gellrich, N.C.; Alexander, S.; Beat, H.; Sergio, R.; Daniel, C.; Wolf, L.; Rainer, S. Computer-assisted secondary reconstruction of unilateral posttraumatic orbital deformity. *Plast. Reconstr. Surg.* **2002**, *110*, 1417–1429. [PubMed]
6. Ewers, R.; Schicho, K.; Undt, G.; Wanschitz, F.; Truppe, M.; Seemann, R.; Wagner, A. Basic research and 12 years of clinical experience in computer-assisted navigation technology: A review. *Int. J. Oral Maxillofac. Surg.* **2005**, *34*, 1–8. [CrossRef] [PubMed]
7. Saito, J.; Kaneko, M.; Ishikawa, Y.; Yokoyama, U. Challenges and Possibilities of Cell-Based Tissue-Engineered Vascular Grafts. *Cyborg Bionic Syst.* **2021**, *2021*, 1532103. [CrossRef]
8. Yi, H.; Kim, S.; Kim, M.; Kim, J.; Jeon, J.S.; Park, J. Bioprinting methods for fabricating in vitro tubular blood vessel models. *Cyborg Bionic Syst.* **2023**, *in press*.
9. Khoury, R.L.; Nagiah, N.; Mudloff, J.A.; Thakur, V.; Chattopadhyay, M.; Joddar, B. 3D Bioprinted Spheroidal Droplets for Engineering the Heterocellular Coupling between Cardiomyocytes and Cardiac Fibroblasts. *Cyborg Bionic Syst.* **2021**, *2021*, 9864212. [CrossRef]
10. Kim, Y.C.; Jeong, W.S.; Park, T.K.; Choi, J.W.; Koh, K.S.; Oh, T.S. The accuracy of patient specific implant prebented with 3D-printed rapid prototype model for orbital wall reconstruction. *J. Cranio-Maxillofac. Surg.* **2017**, *45*, 28–36. [CrossRef]
11. Kang, S.; Kwon, J.Y.; Ahn, C.J.; Esmaeli, B.; Kim, G.B.; Kim, N.K.; Sa, H.S. Generation of customized orbital implant templates using 3-dimensional printing for orbital wall reconstruction. *Eye* **2018**, *32*, 1864–1870. [CrossRef] [PubMed]
12. Vehmeijer, M.; Eijnatten, M.V.; Iberton, N.L.; Wolff, J. A novel method of orbital floor reconstruction using virtual planning, 3-dimensional printing, and autologous bone. *J. Oral Maxillofac. Surg.* **2016**, *74*, 1608–1612. [CrossRef] [PubMed]
13. Bin, F.; Han, C.; Sun, Y.J.; Wang, B.F.; Lin, C.; Liu, S.Y.; Li, G.Y. Clinical effects of 3-D printing-assisted personalized reconstructive surgery for blowout orbital fractures. *Graefe's Arch. Clin. Exp. Ophthalmol.* **2017**, *255*, 2051–2057.
14. Stoor, P.; Suomalainen, A.; Lindqvist, C.; Mesimaki, K.; Danielsson, D.; Westermark, A.; Kontio, R.K. Rapid prototyped patient specific implants for reconstruction of orbital wall defects. *J. Cranio-Maxillofac. Surg.* **2014**, *42*, 1644–1649. [CrossRef] [PubMed]
15. Jin, H.R.; Shin, S.O.; Choo, M.J.; Choi, Y.S. Relationship between the extent of fracture and the degree of enophthalmos in isolated blowout fractures of the medial orbital wall. *J. Oral Maxillofac. Surg.* **2000**, *58*, 617–620. [CrossRef] [PubMed]
16. Ploder, O.; Klug, C.; Voracek, M.; Burggasser, G.; Czerny, C. Evaluation of computer-based area and volume measurement from coronal computed tomography scans in isolated fractures of the orbital floor. *J. Oral Maxillofac. Surg.* **2002**, *60*, 1267–1272. [CrossRef]
17. Zhang, Z.; Zhang, Y.; He, Y.; An, J.; Zwahlen, R.A. Correlation between volume of herniated orbital contents and the amount of enophthalmos in orbital floor and wall fractures. *J. Oral Maxillofac. Surg.* **2012**, *70*, 68–73. [CrossRef]
18. Shahrokh, R.; Hamid, R.F.; Kazem, S.K.; Mehdi, H.; Sadaf, A. Customized Titanium Mesh Based on the 3D Printed Model vs. Manual Intraoperative Bending of Titanium Mesh for Reconstructing of Orbital Bone Fracture: A Randomized Clinical Trial. *Rev. Recent Clin. Trials* **2017**, *12*, 154–158.
19. Kim, J.H.; Lee, C.R.; Oh, D.Y.; Jun, Y.J.; Moon, S.H. Comparison of Efficacy between Three-Dimensional Printing and Manual-Bending Implants for Inferomedial Orbital Fracture: A Retrospective Study. *Appl. Sci.* **2021**, *11*, 7971. [CrossRef]
20. William, J.W.; Curtis, J.H.; Alon, K.; Kim, J. Use of 3D Printed Models to Create Molds for Shaping Implants for Surgical Repair of Orbital Fractures. *Acad. Radiol.* **2020**, *27*, 536–542.
21. Jarosław, M.S.; Marlon, S.L.; Szymon, M.; Agastya, P.; Finn, S.; Dmitry, T.; Justyna, F.; Kinga, J.; Mikołaj, F.; Ewa, P.; et al. The Role of 3D Printing in Planning Complex Medical Procedures and Training of Medical Professionals—Cross-Sectional Multispecialty Review. *Int. J. Environ. Res. Public Health* **2022**, *19*, 3331.
22. Lauren, S.; Michelle, H.; Fields, J.M.; Backlund, E.; Robert, P.; Kristy, M.S. Standardizing evaluation of patient-specific 3D printed models in surgical planning: Development of a cross-disciplinary survey tool for physician and trainee feedback. *BMC Med. Educ.* **2022**, *22*, 614.
23. Pang, S.S.Y.; Fang, C.; Chan, J.Y.W. Application of three-dimensional printing technology in orbital floor fracture reconstruction. *Trauma Case Rep.* **2018**, *17*, 23–28. [CrossRef]

24. Wi, J.M.; Sung, K.H.; Chi, M. Orbital volume restoration rate after orbital fracture' a CT-based orbital volume measurement for evaluation of orbital wall reconstructive effect. *Eye* **2017**, *31*, 713–719. [CrossRef] [PubMed]
25. Chiarella, S.; Gaia, G.; Francesca, C.; Davide, G.T.; Alessandro, U.; Virgilio, F.F. Age-and sex-related changes in the soft tissues of the orbital region. *Forensic Sci. Int.* **2009**, *185*, 115.
26. Lee, K.M.; Park, J.U.; Kwon, S.T.; Kim, S.W.; Jeong, E.C. Threedimensional pre-bent titanium implant for concomitant orbital floor and medial wall fractures in an East asian population. *Arch. Plast Surg.* **2014**, *41*, 480–485. [PubMed]
27. Kim, Y.; Park, Y.; Chun, K.J. Considerations for the Management of Medial Orbital Wall Blowout Fracture. *Arch. Plast Surg.* **2016**, *43*, 229–236. [CrossRef]
28. Nazimi, A.J.; Khoo, S.C.; Nabil, S.; Nordin, R.; Lan, T.H.; Rajandram, R.K.; Rajaran, J.R. Intraoperative Computed Tomography Scan for Orbital Fracture Reconstruction. *J. Craniofac. Surg.* **2019**, *30*, 2159–2162. [CrossRef]